

# Empirically Validating Conformal Prediction on Modern Vision Architectures Under Distribution Shift and Long-tailed Data

Kevin Kasa<sup>1,2</sup> Graham W. Taylor<sup>1,2</sup>

## Abstract

Conformal prediction has emerged as a rigorous means of providing deep learning models with reliable uncertainty estimates and safety guarantees. Yet, its performance is known to degrade under distribution shift and long-tailed class distributions, which are often present in real world applications. Here, we characterize the performance of several post-hoc and training-based conformal prediction methods under these settings, providing the first empirical evaluation on large-scale datasets and models. We show that across numerous conformal methods and neural network families, performance greatly degrades under distribution shifts violating safety guarantees. Similarly, we show that in long-tailed settings the guarantees are frequently violated on many classes. Understanding the limitations of these methods is necessary for deployment in real world and safety-critical applications.

## 1. Introduction

Deep learning models have shown the ability to complete a diverse range of tasks with exceedingly high performance (Silver et al., 2017; Brown et al., 2020; Dosovitskiy et al., 2020b). However, high performance metrics (e.g., accuracy) alone are insufficient for deployment in safety-critical applications, where uncertainty measures and safety guarantees that experts can trust are required (Ovadia et al., 2019). *Conformal prediction* (CP) (Vovk et al., 2005) is a promising method for addressing these limitations. Conformal prediction turns heuristic notions of uncertainty into reliable ones through a post-training adjustment, which can then be used to predict *confidence sets* that are guaranteed

<sup>1</sup>School of Engineering, University of Guelph, Guelph, Canada <sup>2</sup>Vector Institute for Artificial Intelligence, Toronto, Canada. Correspondence to: Kevin Kasa <kkasa@uoguelph.ca>.

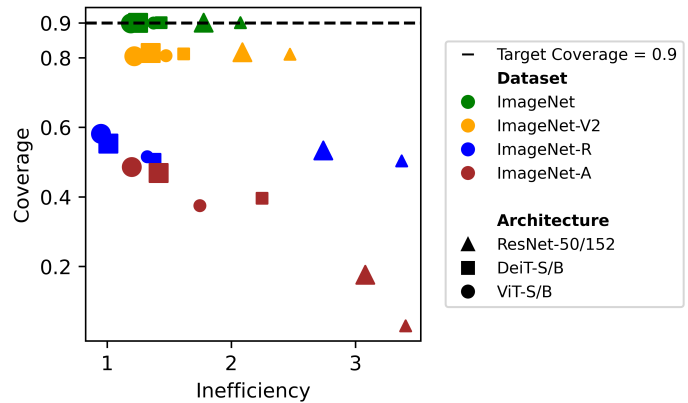


Figure 1: **Performance of threshold conformal prediction (Sadinle et al., 2019) degrades across various neural architectures when tested on distribution-shifted ImageNet datasets.** Target coverage is set to 0.90. All conformal prediction thresholds were first calibrated on a held-out portion of the original validation set. The **same** threshold was used to construct confidence sets in subsequent test sets. Target coverage is consistently violated for all distribution-shifted sets. Likewise, the average confidence set size, or “inefficiency”, is observed to increase under distribution shift. Larger markers reflect larger architectures within the family.

to contain the true class with some user specified error rate.

Various conformal prediction methods (Sadinle et al., 2019; Stutz et al., 2022; Romano et al., 2020; Angelopoulos et al., 2022a; Teng et al., 2023) perform well on a number of complex tasks such as image classification and object detection (Angelopoulos et al., 2022b). However, these results thus far are largely limited to in-distribution and class-balanced data regimes. This is problematic since data encountered in real-world settings is often imbalanced (Krawczyk, 2016) or subject to distribution shift (Castro et al., 2020), and robustness to these settings is necessary for the safe deployment of ML (Amodei et al., 2016).

Despite the importance of understanding performance in these real-world settings, there has thus far been no comprehensive investigation of the performance of popular

conformal prediction methods under distribution shift and long-tailed data. Since conformal prediction assumes identically distributed data and guarantees provided are based on micro- rather than macro-averages, it is unsurprising that performance would degrade under shifted and long-tailed distributions. This phenomenon has been observed in small-scale datasets (Tibshirani et al., 2020). Nonetheless, the recent adoption of conformal prediction into deep learning and safety-critical domains (Angelopoulos et al., 2022b; Muthali et al., 2023; Vazquez & Facelli, 2022; Lu et al., 2022) warrants specific investigation of these methods using modern neural network architectures and large-scale datasets that are more characteristic of data found “in the wild”.

In this study, we evaluate four different conformal prediction methods on numerous distribution-shifted and long-tailed datasets and thoroughly characterize their performance under these conditions. We investigate across three deep learning model families, while also controlling for model size. Our primary findings are:

- Safety guarantees in terms of coverage (Eq. 8) are violated even under small distribution shifts.
- Class-conditional coverage is frequently violated in long-tailed distributions.
- The size of the confidence sets, with smaller being more desirable, increases under both these settings.
- The above results hold across all CP methods and model architectures.

## 2. Methods

In this study, four conformal prediction methods were evaluated across five distribution-shifted datasets and one long-tailed dataset, for image classification tasks. Three neural architecture families were used as the base classifier, to determine their affect on CP performance, which was evaluated using several metrics.

### 2.1. Conformal Prediction Methods

The common classification paradigm involves training a model  $\pi_\theta(x)$  to predict a *single label*  $Y \in [K] := \{1, \dots, K\}$ . In contrast, conformal prediction is a statistical method that can be used to predict confidence *sets* for machine learning models (Angelopoulos et al., 2022a). Formally, it aims to construct a confidence set  $\mathcal{C} \subseteq [K]$  such that the true class is included with some user specified error rate  $\alpha$ :

$$\mathbb{P}(Y_{\text{test}} \in \mathcal{C}(X_{\text{test}})) \geq 1 - \alpha. \quad (1)$$

This is done through a two step post-processing procedure. In the calibration step, a score function  $s(x, y)$  is used on

held-out data to transform a provisional uncertainty measure (e.g., softmax values) into *conformity scores*. The  $1 - \alpha$  quantile of the conformity scores is then used to determine a threshold  $\tau$ . In the prediction step, sets  $\mathcal{C}(X)$  are constructed on new unseen data by including all the labels whose conformity scores fall within the threshold, guaranteeing  $1 - \alpha$  coverage. Importantly, this guarantee is known as *marginal coverage*, since it holds in expectation *unconditionally* across all data points rather than per-class. The returned confidence sets can also be used as an uncertainty estimate, with larger confidence sets  $|\mathcal{C}(X)|$  suggesting greater uncertainty in the predictions.

The **threshold conformal prediction (THR)** method (Sadinle et al., 2019) generally produces the smallest average set sizes. Here, the confidence sets are constructed as:

$$\mathcal{C}(x; \tau) := \{k \in [K] : s(x, k) > \tau\} \quad (2)$$

Here, the score function is defined as  $s(x, y) = \pi_\theta(x)_y$ , and the threshold  $\tau$  is computed as the  $\alpha(1 + 1/N_{\text{cal}})$  quantile of the calibrated conformity scores. During calibration, the softmax value corresponding to the true class  $y$  of the input  $x$  is used in the conformity scores. At test time, this method includes in the set those classes whose softmax score is greater than the calibrated threshold. Although THR produces small set sizes, it may lead to “uneven” coverage, with difficult classes achieving worse coverage.

**Adaptive prediction sets (APS)** (Romano et al., 2020) were developed to improve conditional coverage, with the trade-off of larger set sizes. In the APS method, the conformity scores are calculated by accumulating softmax values:

$$s(x, y) = \sum_{j=1}^y \hat{\pi}_\theta(x)_j, \quad (3)$$

Where  $\hat{\pi}_\theta(x)$  is the sorted softmax values for input  $x$  from greatest to smallest. Subsequently, sets are constructed by including values *less* than the threshold  $\tau$ :

$$\mathcal{C}(x; \tau) := \{k \in [K] : s(x, k) < \tau\}, \quad (4)$$

Similarly to THR, the conformity scores with respect to the true class  $y_i$  are used for calibration, and the  $(1 - \alpha)(1 + 1/N_{\text{cal}})$  quantile is used to find the value  $\tau$  that ensures marginal coverage on test examples.

**Regularized adaptive prediction sets (RAPs)** (Angelopoulos et al., 2022a) build on APS by modifying the conformity scores to include a penalty  $\lambda$  to classes beyond some specified threshold  $k_{\text{reg}}$ . Specifically, the score function is defined as:

$$s(x, y) := \sum_{j=1}^k \pi_{\theta}(x)_y + \lambda \cdot (o_x(y) - k_{\text{reg}})^+, \quad (5)$$

where  $o_x(y)$  is the ranking of label  $y$  among the sorted probabilities, and  $(\cdot)^+$  indicates the positive part of the expression. The confidence sets are then defined the same as in Equation 4. The regularization helps to exclude probabilities that are deep in the tail that would otherwise have been included, since labels now require a greater score to be included in the set. This helps to produce smaller prediction sets than APS (albeit not as small as THR), and has been shown to work well on large datasets like ImageNet (Angelopoulos et al., 2022a). In our experiments, convolution-based networks use values of  $\lambda = 0.01$  and  $k_{\text{reg}} = 5$ , and transformer-based networks use  $\lambda = 0.1$  and  $k_{\text{reg}} = 2$ .

The CP methods described thus far are implemented *after* a model is trained, which does not directly optimize the underlying model to produce high performing confidence sets. **Conformal training (ConfTr)** (Stutz et al., 2022) was proposed to address this, by simulating the conformal prediction process during training. This is done by splitting each training batch  $B$  into a calibration  $B_{\text{cal}}$  and prediction  $B_{\text{pred}}$  subset. Just like in regular CP,  $B_{\text{cal}}$  is used to calibrate the threshold  $\tau$ , and confidence sets are formed on  $B_{\text{pred}}$ . To perform the thresholding step, differentiable sorting (Blondel et al., 2020) is used to find the quantiles of the conformity scores in a way that can be back-propagated during training. The size of the confidence sets is then used as the loss function to be minimized during training:

$$\mathcal{L}_{\text{size}} = \max \left( 0, \sum_{k=1}^K E_{\theta,k}(x; \tau) - \kappa \right). \quad (6)$$

In Equation 6,  $E_{\theta,k}(x; \tau)$  is a “smooth” assignment of class  $k$  to the confidence set, calculated as  $E_{\theta,k}(x; \tau) := \sigma \left( \frac{s(x,y) - \tau}{T} \right)$ , where  $\sigma(\cdot)$  is the Sigmoid function and  $T \in [0, 1]$  is a temperature parameter controlling the smoothness. This penalizes the set sizes, and the hyper-parameter  $\kappa \in \{0, 1\}$  determines whether or not sets of size one are penalized (i.e.,  $\kappa = 1$  means that singleton sets will incur no loss). An additional classification loss can be included to ensure the true label is included in the confidence sets:

$$\mathcal{L}_{\text{class}} = \sum_{k=1}^K [(1 - C_{\theta,k}(x; \tau)) \cdot \mathbf{1}[y = k]]. \quad (7)$$

A weighted combination  $\mathcal{L} = \mathcal{L}_{\text{class}} + \lambda \mathcal{L}_{\text{size}}$  can then be used to train the model.

For this method, a ResNet-50 pre-trained on ImageNet (Wightman, 2019) was used as the base model. The train-

ing methodology and hyper-parameters closely follow that used by the original authors on the CIFAR-100 dataset (Stutz et al., 2022). This included re-initializing the final fully connected layer, and training one baseline model using cross-entropy loss and one with the combined  $\mathcal{L}_{\text{size}}$  and  $\mathcal{L}_{\text{class}}$  losses, defined in Equation 6 and Equation 7.

Any CP method can be used to predict the confidence sets during training, however in practise THR has been shown to produce better results, so that is used in this study for the ConfTr experiments. Because ConfTr relies on smooth sorting / assignment operations, post-training conformal prediction is still performed to ensure the formal guarantees are maintained.

## 2.2. Evaluation Metrics

The primary metrics used for evaluation are coverage and inefficiency. **Coverage** measures the fraction of true labels that are actually included in the confidence set:

$$\text{Cover} := \frac{1}{N_{\text{test}}} \sum_{i=1}^{N_{\text{test}}} \mathbf{1}[y_i \in \mathcal{C}(x_i)]. \quad (8)$$

The conformal prediction process guarantees that  $\mathbb{P}(Y_{\text{test}} \in \mathcal{C}(X_{\text{test}})) \geq 1 - \alpha$ , thus the *Cover* metric should be  $\geq 1 - \alpha$  on average. However, conformal prediction does not guarantee **class conditional coverage**:  $\mathbb{P}(Y_{\text{test}} \in \mathcal{C}(X_{\text{test}}) | Y_{\text{test}} = y) \geq 1 - \alpha$ . We can capture conditional performance using a “macro” coverage metric. First we can consider *Cover(k)* to be the coverage computed only on test points from class  $k \in [K]$ . The macro coverage is then:

$$\text{Macro Cover} := \frac{1}{K} \sum_{k=1}^K \text{Cover}(k). \quad (9)$$

The non-conditional guarantees of conformal prediction mean that although across an entire dataset the desired coverage may be maintained, there may be classes which violate the desired coverage level. This is especially pertinent for long-tailed datasets. Thus, the number of classes that violates the coverage level is found:

$$\text{Cover Violation} := \sum_{k=1}^K \mathbf{1}[\text{Cover}(k) < 1 - \alpha]. \quad (10)$$

**Inefficiency** is a measure of the size of the confidence sets. The prediction sets must both provide adequate coverage (contain the right class), and be *informative*; very large prediction sets are of little use. Inefficiency is measured as:

$$\text{Ineff} := \frac{1}{N_{\text{test}}} \sum_{i=1}^{N_{\text{test}}} |\mathcal{C}(x_i)|. \quad (11)$$

The macro inefficiency is also calculated, to determine if some classes tend to return particularly large sets. Similarly to Equation 9, we define *Ineff(x)* as the inefficiency

on class  $k$ , and the macro inefficiency as:

$$\text{Macro Ineff} := \frac{1}{K} \sum_{k=1}^K \text{Ineff}(k). \quad (12)$$

The macro coverage and inefficiency metrics will be used to characterize performance on the long-tailed datasets.

### 2.3. Datasets

**Distribution Shift.** We use the ImageNet (Deng et al., 2009) dataset to train our neural networks and calibrate the CP classifiers. Following previous works on conformal prediction (Angelopoulos et al., 2022a), we reserve 50% of the ImageNet validation set to find the threshold  $\tau$ . This **same threshold** is used to form prediction sets on the remaining ImageNet validation set, as well as the following distribution-shifted datasets:

1. **ImageNetV2** (Recht et al., 2019) is a new ImageNet test set collected by closely following the same format and collection process as ImageNet, with the goal of mimicking the original data distribution.<sup>1</sup>
2. **ImageNet-C** (Hendrycks & Dietterich, 2018) applies common visual corruptions to the ImageNet validation set. In this study, the Gaussian noise, motion blur, brightness, and contrast corruptions are investigated, representative of the four main categories — noise, blur, weather, and digital, respectively.
3. **ImageNet-A** (Hendrycks et al., 2021b) contains naturally adversarial images that a ResNet-50 incorrectly classifies, but can be correctly classified by humans.
4. **ImageNet-R** (Hendrycks et al., 2021a) consists of rendered versions of ImageNet classes, such as drawings, cartoons, etc.

The details of these datasets are summarized in Table 1. Metrics are reported as the average across ten trials, to account for variation in the calibration split.

**Long-tailed labels.** Conformal prediction performance on long-tailed data distributions was evaluated on the PlantNet-300k dataset (Garcin et al., 2021). This is a highly imbalanced dataset, with 80% of classes accounting for only 11% of the total number of images. In addition to the 243,916 training examples, PlantNet-300k has defined validation and test sets, each with 31,118 examples and at least one image of each class in each set. The validation

<sup>1</sup>It is difficult to conclude whether this dataset represents a true distribution shift in the absence of convincing generalization error bounds for ImageNet-scale DNNs, however, we adopt Recht et al.’s hypothesis that it indeed represents a small shift.

Table 1: Alternate ImageNet-based validation datasets used to evaluate performance under distribution shift. For ImageNet-C, the Gaussian noise, motion blur, brightness, and contrast corruptions are used. The conformal calibration process is **only** conducted on the original ImageNet validation set.

Dataset	Number of Images	Number of Classes
ImageNet-V2 (Recht et al., 2019)	10,000	1,000
ImageNet-C (Hendrycks & Dietterich, 2018)	50,000	1,000
ImageNet-A (Hendrycks et al., 2021b)	7,500	200
ImageNet-R (Hendrycks et al., 2021a)	30,000	200

Table 2: Comparison between using baseline cross-entropy training and ConfTr, which directly optimizes set sizes during training. Although ConfTr leads to smaller sizes on the in-distribution test data, there is negligible difference in coverage between the two methods on ImageNet-V2. Coverage target is 0.99.

Datasets	Accuracy		Coverage		Inefficiency	
	Baseline	ConfTr	Baseline	ConfTr	Baseline	ConfTr
ImageNet	76.91	72.40	0.99	0.99	32.21	29.89
ImageNet-V2	64.68	60.45	0.97	0.97	50.79	46.99

set is used to calibrate the conformal prediction methods and find the threshold, and the test set is used to form confidence sets and evaluate performance. Here, all three data splits (train, validation, and test) are long-tailed, meaning that **the conformal calibration process is conducted on highly imbalanced data**.

### 2.4. Deep Learning Models

To account for differences in model architecture and training algorithms, three distinct model families were evaluated:

1. **ResNets** (He et al., 2015) are prototypical convolutional neural networks.
2. **Vision Transformers (ViT)** (Dosovitskiy et al., 2020a) are transformer-based architectures that are pre-trained on ImageNet-21k (Ridnik et al., 2021), before being fine-tuned on ImageNet-1k.
3. **Data efficient image Transformers (DeiT)** (Touvron et al., 2022) are also transformer networks, however they are trained only on ImageNet-1k following a carefully designed training procedure.

## 3. Experiments and Results

### 3.1. Distribution Shift

Our results on alternate ImageNet test sets are summarized in Figure 1. We can see that the desired coverage is

Table 3: Conformal prediction results on PlantNet-300k. While marginal coverage of 0.90 is maintained, class-conditional coverage is frequently violated. The conformal threshold is calibrated on a (long-tailed) held-out validation set.

Model	CP Method	Accuracy	Macro Acc.	Coverage	Macro Coverage	Inefficiency	Macro Inefficiency	# (%) Violated Classes
ResNet-152	THR	80.84	36.82	0.899	0.505	1.46	1.99	774 (72%)
	APS			0.900	0.648	3.67	13.75	617 (57%)
	RAPS			0.900	0.610	2.15	5.17	665 (62%)
DeiT-B	THR	82.68	43.57	0.898	0.541	1.30	1.50	714 (66%)
	APS			0.900	0.713	4.70	18.30	513 (47%)
	RAPS			0.901	0.603	1.68	2.64	654 (60%)
ViT-B	THR	82.15	35.86	0.899	0.461	1.56	2.42	800 (74%)
	APS			0.899	0.744	12.37	98.45	466 (43%)
	RAPS			0.901	0.551	1.67	3.27	697 (64%)

consistently violated across all models. Distribution shift also leads to increased inefficiency — a proxy for the increased uncertainty of the underlying model. The coverage target is violated even on small distribution shifts, such as ImageNet-V2, which was purposefully and carefully constructed to match the original ImageNet distribution as closely as possible. The inability of these methods to maintain coverage even on minor distribution shifts highlights the risks of deployment in real world situations, without additional safety features.

Smaller models exhibit worse inefficiency, and often lower coverage rates. The larger ViT / DeiT models perform best overall with the smallest degradation under distribution shift. These results highlight the value of combining conformal prediction with modern, high-performing deep learning models. It affirms that efforts to improve the performance of the base model may improve the performance of conformal prediction methods under distribution shift. Refer to Appendix A for detailed results on these datasets, as well as ImageNet-C results at each corruption level. Further, Appendix D shows the relationship between model accuracy and CP coverage, and Appendix E includes results on the recent ImageNet-W (Li et al., 2023) dataset.

Table 2 shows the results of the conformal training method. As expected, the ConfTr method leads to smaller sets on the in-distribution data, however, this does not translate to improved coverage on distribution-shifted data.

### 3.2. Long-tailed Label Distributions

Table 3 shows the results on the long-tailed PlantNet-300k dataset. Although the target coverage of 0.90 is maintained marginally across the entire dataset, it is frequently violated on a class-conditional basis. Indeed, there are often hundreds of classes with violated coverage levels, leading to a violation of coverage on up to 70% of the classes in the worst case. This is consistent across all models and methods, and highlights the difficulty of applying conformal prediction methods to long-tailed data distributions.

The ineffectiveness of approximating class-conditional coverage on PlantNet-300k is further demonstrated in the Appendix (see Table 6). The Appendix also includes the results of experiments on the iNaturalist-2018 (iNaturalist 2018 competition dataset) and -2019 (iNaturalist 2019 competition dataset) datasets (see Table 7).

## 4. Conclusion

In this paper, we studied the performance of conformal prediction methods under distribution shift and long-tailed data, on large-scale datasets and modern neural architectures. We show that performance degrades in these regimes, and coverage guarantees are frequently violated. We also observed increased inefficiency, the average size of the conformal sets. While violation of coverage guarantees is undesirable, inefficiency indicates model uncertainty. A good model should exhibit heightened uncertainty with OOD examples.

There have been several recent methods developed in dealing with distribution shift (Amoukou & Brunel, 2023; Gendler et al., 2022; Gibbs & Candès, 2022; Barber et al., 2023; Dunn et al., 2022; Bhatnagar et al., 2023; Cauchois et al.; Gibbs et al., 2023) and class-conditional coverage (Deng et al., 2023; Fisch et al., 2021; Jung et al., 2022). However, these have thus far been developed mostly on small-scale datasets, and it remains to be seen how they translate to the large-scale datasets studied here. This is something future works may tackle, and we hope that our results will serve as baselines upon which new conformal prediction methods and novel algorithms and architectures for deep learning can improve.

Ultimately, this work highlights the challenges that conformal prediction methods may face in real world applications, where class imbalance is common and data distributions are ever-shifting. Developing and empirically evaluating conformal prediction methods that are more robust to these admittedly difficult settings is a key requirement to their adoption in safety-critical environments.

## References

- Amodei, D., Olah, C., Steinhardt, J., Christiano, P., Schulman, J., and Mané, D. Concrete problems in ai safety, 2016. **1**
- Amoukou, S. I. and Brunel, N. J. B. Adaptive Conformal Prediction by Reweighting Nonconformity Score, March 2023. URL <http://arxiv.org/abs/2303.12695>. arXiv:2303.12695 [cs, stat]. **5**
- Angelopoulos, A., Bates, S., Malik, J., and Jordan, M. I. Uncertainty Sets for Image Classifiers using Conformal Prediction, September 2022a. URL <http://arxiv.org/abs/2009.14193>. arXiv:2009.14193 [cs, math, stat]. **1, 2, 3, 4**
- Angelopoulos, A. N., Bates, S., Candès, E. J., Jordan, M. I., and Lei, L. Learn then Test: Calibrating Predictive Algorithms to Achieve Risk Control, September 2022b. URL <http://arxiv.org/abs/2110.01052>. arXiv:2110.01052 [cs, stat]. **1, 2**
- Barber, R. F., Candès, E. J., Ramdas, A., and Tibshirani, R. J. Conformal prediction beyond exchangeability, February 2023. URL <http://arxiv.org/abs/2202.13415>. arXiv:2202.13415 [stat]. **5**
- Bhatnagar, A., Wang, H., Xiong, C., and Bai, Y. Improved Online Conformal Prediction via Strongly Adaptive Online Learning, February 2023. URL <http://arxiv.org/abs/2302.07869>. arXiv:2302.07869 [cs, math, stat]. **5**
- Blondel, M., Teboul, O., Berthet, Q., and Djolonga, J. Fast differentiable sorting and ranking, 2020. **3**
- Brown, T. B., Mann, B., Ryder, N., Subbiah, M., Kaplan, J., Dhariwal, P., Neelakantan, A., Shyam, P., Sastry, G., Askell, A., Agarwal, S., Herbert-Voss, A., Krueger, G., Henighan, T., Child, R., Ramesh, A., Ziegler, D. M., Wu, J., Winter, C., Hesse, C., Chen, M., Sigler, E., Litwin, M., Gray, S., Chess, B., Clark, J., Berner, C., McCandlish, S., Radford, A., Sutskever, I., and Amodei, D. Language models are few-shot learners. *CoRR*, abs/2005.14165, 2020. URL <https://arxiv.org/abs/2005.14165>. **1**
- Castro, D. C., Walker, I., and Glocker, B. Causality matters in medical imaging. *Nature Communications*, 11(1), jul 2020. doi: 10.1038/s41467-020-17478-w. URL <https://doi.org/10.1038/s41467-020-17478-w>. **1**
- Cauchois, M., Gupta, S., and Duchi, J. C. Knowing what You Know: valid and validated confidence sets in multi-class and multilabel prediction. **5**
- Deng, J., Dong, W., Socher, R., Li, L.-J., Li, K., and Fei-Fei, L. Imagenet: A large-scale hierarchical image database. In *2009 IEEE conference on computer vision and pattern recognition*, pp. 248–255. Ieee, 2009. **4**
- Deng, S., Ardeshir, N., and Hsu, D. Group conditional validity via multi-group learning, March 2023. URL <http://arxiv.org/abs/2303.03995>. arXiv:2303.03995 [cs, math, stat] version: 1. **5**
- Dosovitskiy, A., Beyer, L., Kolesnikov, A., Weissenborn, D., Zhai, X., Unterthiner, T., Dehghani, M., Minderer, M., Heigold, G., Gelly, S., Uszkoreit, J., and Houlsby, N. An image is worth 16x16 words: Transformers for image recognition at scale. *ArXiv*, abs/2010.11929, 2020a. **4**
- Dosovitskiy, A., Beyer, L., Kolesnikov, A., Weissenborn, D., Zhai, X., Unterthiner, T., Dehghani, M., Minderer, M., Heigold, G., Gelly, S., Uszkoreit, J., and Houlsby, N. An image is worth 16x16 words: Transformers for image recognition at scale. *CoRR*, abs/2010.11929, 2020b. URL <https://arxiv.org/abs/2010.11929>. **1**
- Dunn, R., Wasserman, L., and Ramdas, A. Distribution-Free Prediction Sets for Two-Layer Hierarchical Models, February 2022. URL <http://arxiv.org/abs/1809.07441>. arXiv:1809.07441 [math, stat]. **5**
- Fisch, A., Schuster, T., Jaakkola, T., and Barzilay, R. Few-shot Conformal Prediction with Auxiliary Tasks, July 2021. URL <http://arxiv.org/abs/2102.08898>. arXiv:2102.08898 [cs]. **5**
- Garcin, C., Joly, A., Bonnet, P., Affouard, A., Lombardo, J., Chouet, M., Servajean, M., Lorieul, T., and Salmon, J. Pl@ntNet-300K: a plant image dataset with high label ambiguity and a long-tailed distribution. In *NeurIPS Datasets and Benchmarks 2021*, 2021. **4**
- Gendler, A., Weng, T.-W., Daniel, L., and Romano, Y. ADVERSARIALY ROBUST CONFORMAL PREDICTION. 2022. **5**
- Gibbs, I. and Candès, E. Conformal Inference for Online Prediction with Arbitrary Distribution Shifts, October 2022. URL <http://arxiv.org/abs/2208.08401>. arXiv:2208.08401 [cs, stat]. **5**
- Gibbs, I., Cherian, J. J., and Candès, E. J. Conformal prediction with conditional guarantees, 2023. **5**
- He, K., Zhang, X., Ren, S., and Sun, J. Deep residual learning for image recognition. *2016 IEEE Conference on Computer Vision and Pattern Recognition (CVPR)*, pp. 770–778, 2015. **4**

- Hendrycks, D. and Dietterich, T. G. Benchmarking neural network robustness to common corruptions and perturbations. *ArXiv*, abs/1903.12261, 2018. 4
- Hendrycks, D., Basart, S., Mu, N., Kadavath, S., Wang, F., Dorundo, E., Desai, R., Zhu, T., Parajuli, S., Guo, M., Song, D., Steinhardt, J., and Gilmer, J. The many faces of robustness: A critical analysis of out-of-distribution generalization. *ICCV*, 2021a. 4
- Hendrycks, D., Zhao, K., Basart, S., Steinhardt, J., and Song, D. Natural adversarial examples. *CVPR*, 2021b. 4
- iNaturalist 2018 competition dataset. iNaturalist 2018 competition dataset. [https://github.com/visipedia/inat\\_comp/tree/master/2018](https://github.com/visipedia/inat_comp/tree/master/2018), 2018. 5, 8
- iNaturalist 2019 competition dataset. iNaturalist 2019 competition dataset. [https://github.com/visipedia/inat\\_comp/tree/master/2019](https://github.com/visipedia/inat_comp/tree/master/2019), 2019. 5, 8
- Jung, C., Noarov, G., Ramalingam, R., and Roth, A. Batch Multivald Conformal Prediction, September 2022. URL <http://arxiv.org/abs/2209.15145>. arXiv:2209.15145 [cs, math, stat]. 5
- Krawczyk, B. Learning from imbalanced data: open challenges and future directions. *Progress in Artificial Intelligence*, 5:221 – 232, 2016. 1
- Li, Z., Evtimov, I., Gordo, A., Hazirbas, C., Hassner, T., Ferrer, C. C., Xu, C., and Ibrahim, M. A whac-a-mole dilemma: Shortcuts come in multiples where mitigating one amplifies others. June 2023. URL <https://arxiv.org/abs/2212.04825>. 5, 10, 13
- Lu, C., Angelopoulos, A. N., and Pomerantz, S. Improving trustworthiness of ai disease severity rating in medical imaging with ordinal conformal prediction sets. In Wang, L., Dou, Q., Fletcher, P. T., Speidel, S., and Li, S. (eds.), *Medical Image Computing and Computer Assisted Intervention – MICCAI 2022*, pp. 545–554, Cham, 2022. Springer Nature Switzerland. ISBN 978-3-031-16452-1. 2
- Muthali, A., Shen, H., Deglurkar, S., Lim, M. H., Roelofs, R., Faust, A., and Tomlin, C. Multi-agent reachability calibration with conformal prediction, 2023. 2
- Ovadia, Y., Fertig, E., Ren, J., Nado, Z., Sculley, D., Nowozin, S., Dillon, J. V., Lakshminarayanan, B., and Snoek, J. Can you trust your model’s uncertainty? evaluating predictive uncertainty under dataset shift, 2019. 1
- Recht, B., Roelofs, R., Schmidt, L., and Shankar, V. Do imagenet classifiers generalize to imagenet? In *International Conference on Machine Learning*, 2019. 4
- Ridnik, T., Ben-Baruch, E., Noy, A., and Zelnik-Manor, L. Imagenet-21k pretraining for the masses, 2021. 4
- Romano, Y., Sesia, M., and Candès, E. J. Classification with Valid and Adaptive Coverage, June 2020. URL <http://arxiv.org/abs/2006.02544>. arXiv:2006.02544 [stat]. 1, 2
- Sadinle, M., Lei, J., and Wasserman, L. Least Ambiguous Set-Valued Classifiers with Bounded Error Levels. *Journal of the American Statistical Association*, 114(525): 223–234, January 2019. ISSN 0162-1459, 1537-274X. doi: 10.1080/01621459.2017.1395341. URL <http://arxiv.org/abs/1609.00451>. arXiv:1609.00451 [cs, stat]. 1, 2, 8
- Silver, D., Schrittwieser, J., Simonyan, K., Antonoglou, I., Huang, A., Guez, A., Hubert, T., Baker, L., Lai, M., Bolton, A., Chen, Y., Lillicrap, T., Hui, F., Sifre, L., van den Driessche, G., Graepel, T., and Hassabis, D. Mastering the game of go without human knowledge. *Nature*, 550:354–, October 2017. URL <http://dx.doi.org/10.1038/nature24270>. 1
- Stutz, D., Krishnamurthy, Dvijotham, Cemgil, A. T., and Doucet, A. Learning Optimal Conformal Classifiers, May 2022. URL <http://arxiv.org/abs/2110.09192>. arXiv:2110.09192 [cs, stat]. 1, 3
- Teng, J., Wen, C., Zhang, D., Bengio, Y., Gao, Y., and Yuan, Y. Predictive inference with feature conformal prediction, 2023. 1
- Tibshirani, R. J., Barber, R. F., Candès, E. J., and Ramdas, A. Conformal prediction under covariate shift, 2020. 2
- Touvron, H., Cord, M., and J’egou, H. Deit iii: Revenge of the vit. In *European Conference on Computer Vision*, 2022. 4
- Vazquez, J. and Facelli, J. C. Conformal prediction in clinical medical sciences. *Journal of Healthcare Informatics Research*, 6(3):241–252, 2022. doi: 10.1007/s41666-021-00113-8. 2
- Vovk, V. Conditional validity of inductive conformal predictors, 2012. 8
- Vovk, V., Gammerman, A., and Shafer, G. *Algorithmic Learning in a Random World*. 01 2005. doi: 10.1007/b106715. 1
- Wightman, R. Pytorch image models. <https://github.com/rwightman/pytorch-image-models>, 2019. 3

## A. Detailed Results on ImageNet Distribution Shift

The detailed results on alternate ImageNet test sets are reported in Table 4. As mentioned, the target coverage level of 0.90 is violated in nearly all circumstances. We see that THR indeed provides the smallest set sizes, while the adaptability of RAPS generally results in better, but imperfect, coverage. Further, the basic APS method often leads to impractically large set sizes. In addition to degrading coverage, the inefficiency also increases on these datasets; a proxy for the increased uncertainty of the underlying model.

Table 5 further highlights the brittleness of conformal prediction methods. Here, we can see that even minor corruption levels frequently lead to a violation of the target coverage. This is especially noticeable in the combination of smaller networks such as ResNet-50 and the THR method, where the smallest corruption level leads to coverage violations across all corruption types. We can also see that some corruption types lead to a greater degradation than others: motion blur tends to perform worse on average and brightness the best. In spite of the frequent degradation, the combination of DeiT-B / ViT-B and the RAPS algorithm performs consistently better across many settings, maintaining coverage levels only a few percent below the target up to corruption level 3 on most datasets.

## B. Ineffectiveness of class-balanced CP on PlantNet-300k

As demonstrated in Table 3, performing conformal prediction on long-tailed data leads to large violations in class-conditional coverage. Class-conditional coverage can be approached through **class balanced** conformal prediction, which aims to ensure that the specified error rates are guaranteed for *every* class. Sadinle et al. (2019) propose a method that calibrates a threshold for each class, then including classes in the confidence set based on their class-specific thresholds:

$$C(x; \tau) = \left\{ k \in [K] : s(x, k) < \tau^{(k)} \right\}. \quad (13)$$

This method can be used in conjunction with the other post-hoc CP methods described in Appendix ??.

We investigated class-conditional conformal prediction on PlantNet-300k, and summarize the results in Table 6. It results in better macro-coverage and fewer coverage violations than the regular conformal prediction, yet it still leads to class-conditional coverage violations. This is partly because CP coverage holds in expectation across an infinite test set. Where ample data per class is available, like on ImageNet, this can be simulated by repeated random data splits. PlantNet-300k has fixed calibration / test sets and as noted, some classes have very little representation. Further, coverage follows a Beta distribution with  $\alpha$  and  $\beta$  terms reliant on the validation set size (Vovk, 2012), thus a smaller calibration set leads to greater variance in coverage across the (infinite) test set. Thus, when class-balanced conformal prediction is performed on PlantNet-300k, both *the calibration and test sets for each class are very small* due to the long-tailed label distribution. This leads to a high class-conditional variance in coverage and thus does not resolve the coverage violations.

Although this is a challenging setting, it is nonetheless reflective of possible scenarios that can be encountered in the real world. One may imagine many data-constrained environments such as medicine where gathering a large number of examples for rare (yet still important) classes is a challenging feat. If conformal prediction is to be deployed in these settings, this is a hurdle that must be addressed.

## C. iNaturalist Results

The iNaturalist-2018 (iNaturalist 2018 competition dataset) and iNaturalist-2019 (iNaturalist 2019 competition dataset) datasets both feature long-tailed training sets and class-balanced test sets. They are comprised of 8,142 and 1,010 classes, respectively. Here, 50% of the test set is used to calibrate the conformal threshold, and the remainder is used to predict confidence sets. Unlike the PlantNet-300k dataset, the conformal calibration process is conducted on a class-balanced dataset. We can see in Table 7 that this results in a considerably lower percentage of classes with violated coverage.

## D. The Relationship between Accuracy and Coverage

Figure 2 plots the relation between coverage / inefficiency performance and the accuracy of the underlying model, on on the different distribution-shifted datasets. We can observe that coverage generally increases along with accuracy. Inefficiency also improves, albeit the THR method seems to have larger inefficiency improvements.

Similarly, Figure 3 plots the coverage / inefficiency relation with accuracy for various corruption levels and types. There is



Table 4: Performance of various conformal prediction and neural architectures on distribution-shifted ImageNet datasets with a target coverage of 0.90. All conformal prediction thresholds were first calibrated on a held-out portion of the original validation set. The **same** threshold was used for constructing confidence sets in the subsequent test sets. Target coverage is consistently violated for all distribution-shifted sets. Likewise, the average confidence set size, a.k.a. “inefficiency”, is observed to increase under distribution shift.

(a) Performance on original ImageNet validation set

Model	Accuracy	Coverage			Inefficiency		
		THR	APS	RAPS	THR	APS	RAPS
ResNet-50	76.14	0.899	0.899	0.899	2.05	9.06	3.78
ResNet-152	78.04	0.900	0.900	0.900	1.79	6.37	2.98
DeiT-S	81.29	0.900	0.900	0.900	1.42	90.53	2.09
DeiT-B	83.78	0.899	0.898	0.899	1.24	11.59	1.59
ViT-S	81.30	0.899	0.899	0.899	1.37	4.53	1.72
ViT-B	84.61	0.900	0.900	0.899	1.19	4.64	1.54

(b) Performance on ImageNet-V2

Model	Accuracy	Coverage			Inefficiency		
		THR	APS	RAPS	THR	APS	RAPS
ResNet-50	63.15	0.809	0.863	0.766	2.46	15.80	2.25
ResNet-152	66.95	0.815	0.861	0.782	2.08	11.60	2.01
DeiT-S	70.70	0.811	0.901	0.840	1.61	133.04	2.64
DeiT-B	73.28	0.813	0.877	0.838	1.344	18.15	1.89
ViT-S	70.32	0.807	0.872	0.831	1.48	8.17	2.09
ViT-B	74.00	0.805	0.877	0.843	1.22	9.10	1.89

(c) Performance on ImageNet-R

Model	Accuracy	Coverage			Inefficiency		
		THR	APS	RAPS	THR	APS	RAPS
ResNet-50	36.16	0.504	0.710	0.489	3.37	26.55	3.49
ResNet-152	41.33	0.534	0.723	0.528	2.74	22.72	3.14
DeiT-S	45.96	0.508	0.851	0.588	1.39	73.53	5.25
DeiT-B	53.44	0.554	0.809	0.626	1.01	43.12	3.66
ViT-S	46.05	0.516	0.777	0.592	1.32	26.30	3.59
ViT-B	56.84	0.581	0.836	0.679	0.95	27.47	3.20

(d) Performance on ImageNet-A

Model	Accuracy	Coverage			Inefficiency		
		THR	APS	RAPS	THR	APS	RAPS
ResNet-50	0.03	0.029	0.203	0.020	3.08	16.13	3.08
ResNet-152	5.95	0.176	0.402	0.165	3.08	15.86	3.05
DeiT-S	25.95	0.396	0.828	0.519	2.25	69.38	5.19
DeiT-B	38.80	0.469	0.745	0.591	1.41	30.66	3.27
ViT-S	26.75	0.375	0.673	0.478	1.75	13.95	3.29
ViT-B	43.05	0.486	0.803	0.636	1.20	16.39	3.13

(e) Average performance on ImageNet-C – contrast

Model	Accuracy	Coverage			Inefficiency		
		THR	APS	RAPS	THR	APS	RAPS
ResNet-50	35.68	0.512	0.878	0.528	2.66	177.81	4.89
ResNet-152	39.39	0.528	0.844	0.541	2.27	137.79	4.27
DeiT-S	69.10	0.795	0.927	0.842	1.61	143.79	3.35
DeiT-B	72.87	0.765	0.984	0.892	1.13	216.36	4.37
ViT-S	55.23	0.626	0.899	0.719	1.25	90.40	3.79
ViT-B	65.09	0.682	0.913	0.794	1.04	82.53	3.20

(f) Average performance on ImageNet-C – brightness

Model	Accuracy	Coverage			Inefficiency		
		THR	APS	RAPS	THR	APS	RAPS
ResNet-50	64.99	0.827	0.902	0.797	2.52	28.38	2.53
ResNet-152	68.90	0.842	0.904	0.817	2.13	21.39	2.23
DeiT-S	76.16	0.860	0.917	0.883	1.53	131.98	2.58
DeiT-B	78.97	0.862	0.915	0.888	1.30	22.78	1.96
ViT-S	75.20	0.869	0.895	0.876	1.44	8.34	2.01
ViT-B	79.27	0.856	0.899	0.878	1.22	8.26	1.78

(g) Average performance on ImageNet-C – Gaussian noise

Model	Accuracy	Coverage			Inefficiency		
		THR	APS	RAPS	THR	APS	RAPS
ResNet-50	32.94	0.485	0.815	0.487	2.94	114.90	4.40
ResNet-152	42.10	0.573	0.839	0.576	2.55	85.40	3.64
DeiT-S	61.45	0.727	0.940	0.801	1.67	236.23	3.96
DeiT-B	68.77	0.756	0.945	0.837	1.28	84.12	3.03
ViT-S	58.31	0.677	0.887	0.748	1.43	40.84	3.09
ViT-B	67.40	0.728	0.912	0.817	1.16	34.06	2.65

(h) Average performance on ImageNet-C – motion blur

Model	Accuracy	Coverage			Inefficiency		
		THR	APS	RAPS	THR	APS	RAPS
ResNet-50	36.19	0.528	0.864	0.543	3.10	117.77	4.54
ResNet-152	45.20	0.609	0.873	0.624	2.51	80.87	3.68
DeiT-S	55.30	0.664	0.933	0.746	1.75	253.38	4.25
DeiT-B	63.01	0.706	0.897	0.777	1.34	43.27	2.73
ViT-S	59.23	0.687	0.884	0.756	1.46	30.51	3.00
ViT-B	66.56	0.718	0.894	0.801	1.16	27.10	2.56

Table 5: Coverage on four different corruption types from the ImageNet-C dataset. The coverage target of 0.90 is frequently violated even with minor levels of corruption.

Model	CP Method	Contrast					Brightness					Gaussian Blur					Motion Blur				
		1	2	3	4	5	1	2	3	4	5	1	2	3	4	5	1	2	3	4	5
ResNet-50	THR	0.808	0.753	0.627	0.300	0.073	0.871	0.860	0.840	0.809	0.756	0.779	0.687	0.524	0.314	0.115	0.809	0.714	0.533	0.339	0.245
	RAPS	0.780	0.734	0.632	0.360	0.137	0.832	0.822	0.807	0.783	0.741	0.845	0.797	0.692	0.538	0.326	0.786	0.711	0.553	0.378	0.288
ResNet-152	THR	0.823	0.773	0.657	0.320	0.066	0.880	0.871	0.854	0.826	0.780	0.808	0.747	0.627	0.444	0.213	0.852	0.771	0.638	0.460	0.340
	RAPS	0.800	0.760	0.661	0.368	0.117	0.847	0.839	0.827	0.804	0.768	0.862	0.829	0.767	0.642	0.432	0.882	0.763	0.652	0.500	0.390
DeiT-S	THR	0.867	0.859	0.840	0.778	0.633	0.881	0.876	0.867	0.851	0.825	0.853	0.829	0.772	0.673	0.497	0.852	0.802	0.698	0.540	0.429
	RAPS	0.887	0.880	0.870	0.835	0.735	0.893	0.891	0.887	0.879	0.865	0.885	0.872	0.838	0.777	0.648	0.882	0.853	0.783	0.656	0.559
DeiT-B	THR	0.853	0.845	0.825	0.750	0.551	0.880	0.878	0.868	0.854	0.834	0.857	0.836	0.793	0.722	0.578	0.851	0.814	0.739	0.612	0.513
	RAPS	0.930	0.927	0.919	0.887	0.797	0.894	0.893	0.892	0.887	0.874	0.887	0.886	0.869	0.828	0.738	0.873	0.851	0.801	0.709	0.630
ViT-S	THR	0.844	0.820	0.761	0.542	0.163	0.877	0.871	0.859	0.838	0.805	0.842	0.807	0.737	0.609	0.381	0.845	0.803	0.716	0.582	0.488
	RAPS	0.869	0.856	0.828	0.697	0.349	0.886	0.882	0.874	0.861	0.841	0.867	0.849	0.802	0.714	0.535	0.868	0.843	0.785	0.688	0.610
ViT-B	THR	0.853	0.838	0.801	0.637	0.280	0.877	0.872	0.863	0.846	0.822	0.848	0.821	0.771	0.683	0.523	0.852	0.819	0.747	0.632	0.542
	RAPS	0.880	0.874	0.862	0.804	0.551	0.888	0.886	0.881	0.874	0.862	0.885	0.878	0.856	0.807	0.696	0.881	0.864	0.824	0.752	0.684

Table 6: Class-balanced conformal prediction results on PlantNet-300k. Although this leads to better macro-coverage results than regular (marginal) CP, class-conditional coverage is still violated due to the high coverage variance associated with the small, and fixed, per-class calibration / test set sizes

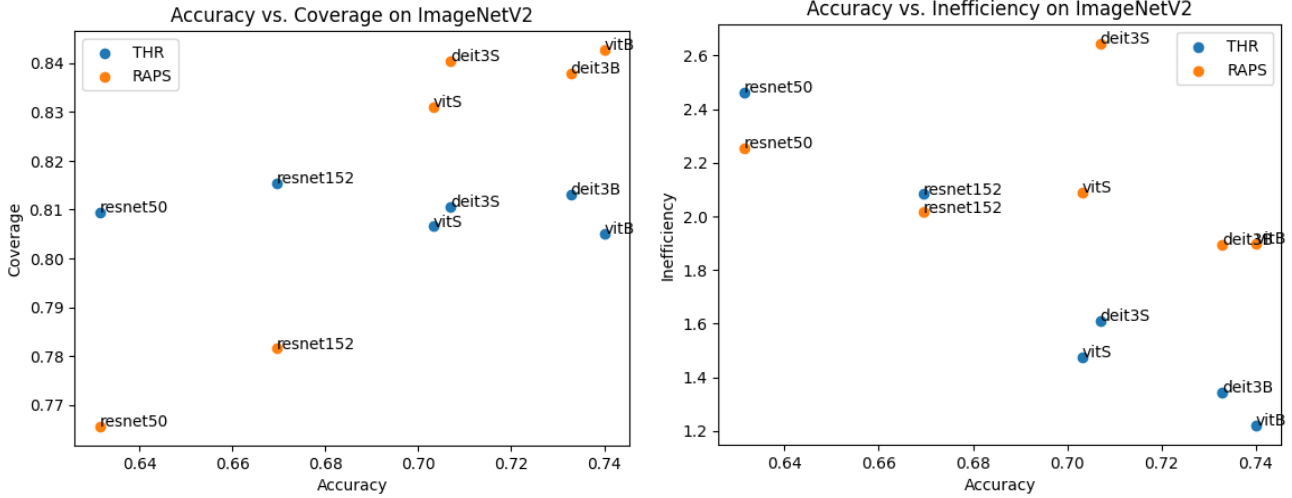
Model	CP Method	Coverage	Macro Coverage	Inefficiency	Macro Inefficiency	# (%) Violated Classes
ResNet-152	THR	0.920	0.676	12.66	29.10	460 (43%)
	APS	0.998	0.983	643.50	737.12	24 (2%)
	RAPS	0.978	0.802	25.10	27.93	268 (25%)
DeiT-B	THR	0.901	0.747	13.56	22.36	372 (34%)
	APS	0.998	0.979	689.90	682.48	27 (2%)
	RAPS	0.968	0.836	16.00	22.47	259 (24%)
ViT-B	THR	0.916	0.659	10.60	43.25	480 (44%)
	APS	0.991	0.951	331.80	656.73	76 (7%)
	RAPS	0.966	0.951	28.75	30.67	360 (33%)

a marked improvement in coverage when the underlying model is more accurate, which seems especially pronounced for greater levels of corruption.

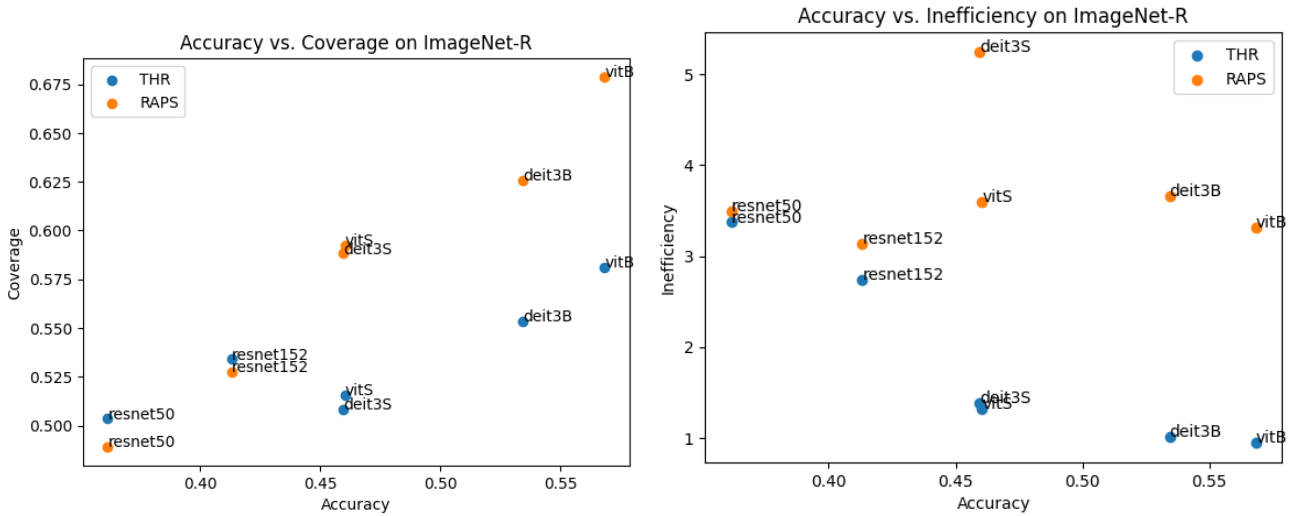
Interestingly, the relation between the accuracy of the underlying neural network and coverage / inefficiency appears to vary with the CP method used. For example, RAPS generally demonstrates a near linear increase in coverage with increased accuracy, however inefficiency gains seem to diminish. Conversely, the inefficiency of the THR algorithm consistently improves with accuracy, and coverage gains are less pronounced.

## E. Results on ImageNet-W

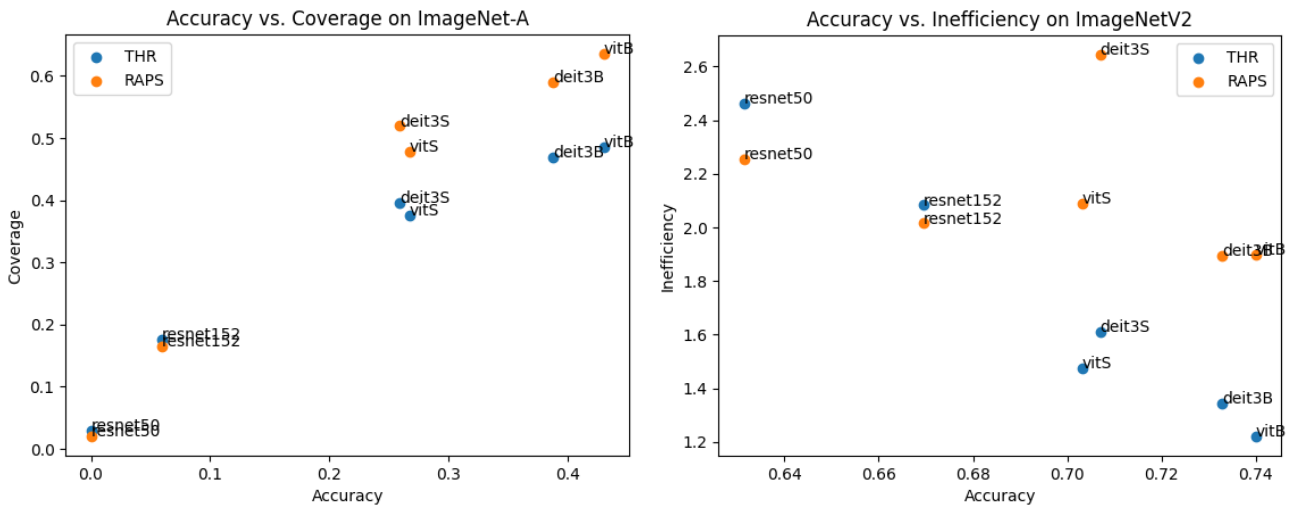
Recent work (Li et al., 2023) has found a reliance on translucent watermarks as a shortcut in current vision models, and the addition of a watermark on the ImageNet validation set leads to large decreases in performance. We investigate this dataset, called ImageNet-W, in the conformal prediction setting and similarly find a general decrease in coverage across most models and methods. As seen in Table 8, the APS method combined with vision transformers is able to maintain coverage on this dataset, at the expense of larger set sizes. This reemphasizes both the brittleness of some conformal prediction methods; a simple watermark is sufficient in violating coverage guarantees, as well as the potential for improvement using better deep learning models and different CP methods.



(a) Coverage (left) and Inefficiency (right) on ImageNetV2

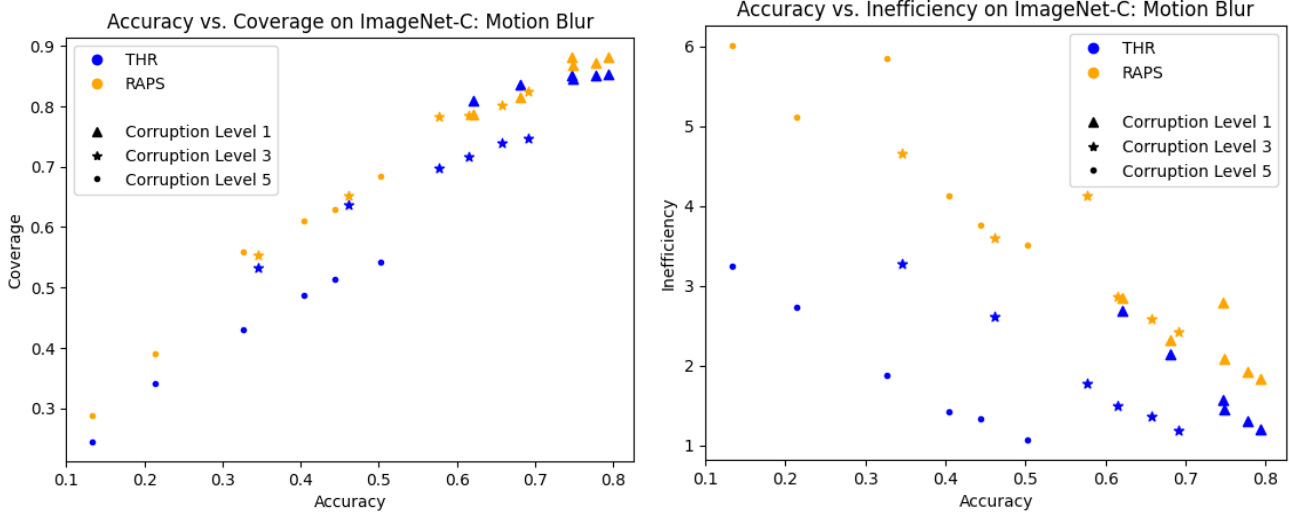


(b) Coverage (left) and Inefficiency (right) on ImageNet-R

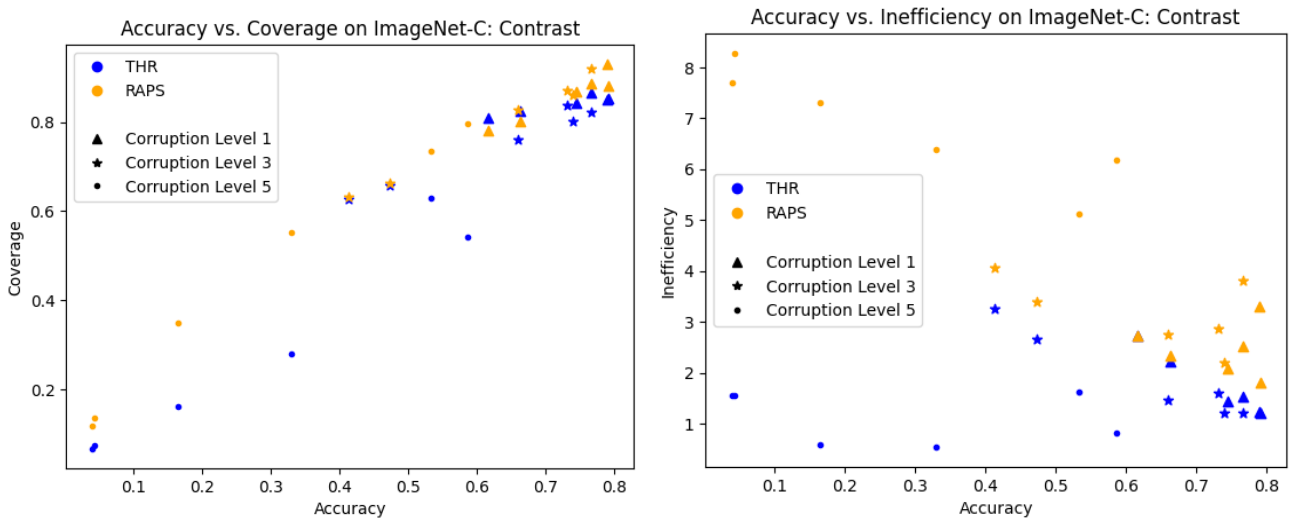


(c) Coverage (left) and Inefficiency (right) on ImageNet-A

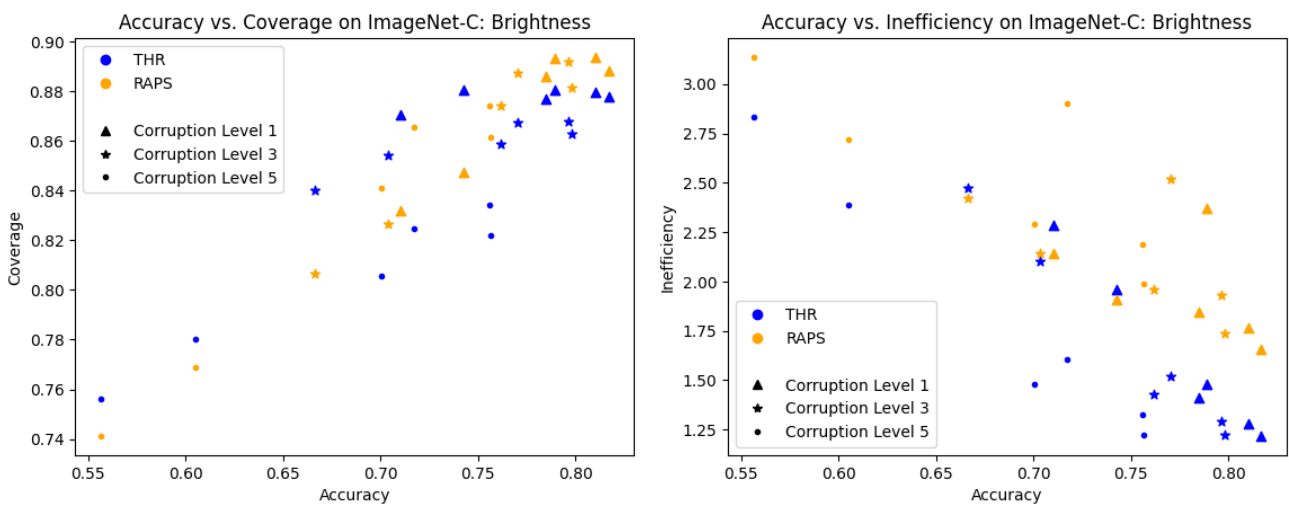
Figure 2: An increase in coverage and inefficiency performance is generally followed by an increase in the accuracy of the underlying model. The target coverage is 0.90 across all datasets.



(a) Coverage (left) and Inefficiency (right) on ImageNet-C — motion blur



(b) Coverage (left) and Inefficiency (right) on ImageNet-C — contrast



(c) Coverage (left) and Inefficiency (right) on ImageNet-C — brightness

Figure 3: Coverage / inefficiency vs. accuracy for various levels of corruption. The target coverage is 0.90.

Table 7: Conformal prediction on iNat-2018 (a) and iNat-2019 (b). Although the conformal thresholds are calibrated on a class-balanced dataset, there is frequent violation of class-conditional coverage.

(a) Conformal prediction results on iNat-2018.

Model	CP Method	Accuracy	Coverage	Inefficiency	Num. (%) Violated Classes
ResNet-152	THR	50.31	0.901	16.39	1,074 (13%)
	RAPS		0.905	16.58	1,078 (13%)
DeiT-B	THR	74.66	0.905	2.82	1,105 (14%)
	RAPS		0.907	3.47	1,093 (13%)
ViT-B	THR	61.61	0.899	7.19	1,119 (14%)
	RAPS		0.899	9.15	1,125 (14%)

(b) Conformal prediction results on iNat-2019.

Model	CP Method	Accuracy	Coverage	Inefficiency	Num. Violated Classes
ResNet-152	THR	62.97	0.900	4.01	113 (11%)
	RAPS		0.900	5.31	147 (15%)
DeiT-B	THR	78.42	0.899	1.58	140 (14%)
	RAPS		0.900	2.03	141 (14%)
ViT-B	THR	75.71	0.900	2.00	146 (14%)
	RAPS		0.904	2.29	146 (14%)

Table 8: Coverage and inefficiency when calibrating on ImageNet and evaluating on ImageNet-W (Li et al., 2023). The target coverage is 0.90.

Model	Accuracy	Coverage			Inefficiency		
		THR	APS	RAPS	THR	APS	RAPS
ResNet-50	48.66	0.657	0.734	0.621	3.07	12.77	2.65
ResNet-152	48.54	0.637	0.741	0.617	2.83	12.21	2.74
DeiT-S	75.41	0.851	0.904	0.872	1.52	111.13	2.53
DeiT-B	78.39	0.855	0.909	0.880	1.28	22.36	1.91
ViT-S	73.86	0.842	0.909	0.873	1.47	9.20	2.21
ViT-B	79.30	0.855	0.912	0.888	1.22	9.01	1.87